Check for updates



# Influence of Transient Thermal Response of Solid Wall on Bubble Dynamics in Pool Boiling

**Liang Zhang[1,3], Zhen-Dong Li[1], Kai Li[1], Hui-Xiong Li[2] and Jian-Fu Zhao[1]***
[1]Key Laboratory of Microgravity (National Microgravity Laboratory)/CAS, Institute of Mechanics, Chinese Academy of Sciences (CAS). Beijing 100190, China
[2]State Key Laboratory of Multiphase Flow in Power Engineering, Xi'an Jiaotong University, Shaanxi 710049, China
[3]State Nuclear Power Software Development Center (SNPSDC). Beijing 102209, China

Received: 20 June 2014; Accepted: 1 September 2014

**Abstract**
Numerical simulation of single bubble pool boiling process including transient thermal response of solid wall is performed using the ghost fluid method and the level set method for the sharp interface representation. The results show that non-physical initial condition in the numerical simulation deeply affects the process of bubble growth, and then multi-cycle simulation is necessary to eliminate its influence. It is shown by the present results that two nucleate criteria, *i.e.* constant waiting time and constant nucleate superheat, for determining the appearance time for the subsequent bubble lead to the same quasi-steady process of bubble growth if they are matched with each other. A periodically expanding and receding thermal "hollow" can be observed inside solid wall underneath the growing bubble. The recovery of the temperature on the nucleate site and the thermal boundary layer near the heating surface is influenced by transient heat conduction inside solid wall, which can affect evidently bubble thermal dynamics and heat transfer.

**Keywords:** Transient Thermal Response, Bubble Growth, Multi-Cycle Simulation, Nucleation Criteria

## NOMENCLATURE

| | |
|---|---|
| $A$ | area |
| $C_p$ | specific heat |
| $D$ | equivalent diameter |
| $\boldsymbol{g}$ | gravity vector |
| $H$ | Heaviside function |
| $h$ | grid size |
| $h_{ev}$ | interfacial thermal resistance |
| $h_{fg}$ | latent heat |
| $k$ | thermal conductivity |
| $L$ | characteristic length |
| $\dot{m}$ | mass flux |
| $\boldsymbol{n}$ | normal vector |
| $p$ | pressure |
| $q$ | heat flux |
| $R_1$ | end position of microlayer |
| $R_0$ | three phase contact point |
| $T$ | temperature |
| $t$ | time |
| $U$ | characteristic velocity |
| $\boldsymbol{u}$ | velocity vector |
| $V$ | Volume |

*Corresponding author. E-mail: jfzhao@imech.ac.cn

**Greece symbols**

| | |
|---|---|
| $\alpha$ | thermal diffusion |
| $\beta_T$ | thermal expansion coefficient |
| $\gamma$ | contact angle |
| $\delta$ | thickness of microlayer |
| $\theta$ | characteristic temperature |
| $\kappa$ | curvature |
| $\mu$ | dynamic viscosity |
| $\nu$ | kinematic viscosity |
| $\rho$ | density |
| $\sigma$ | surface tension |
| $\varphi$ | level set function for vapor-liquid interface |
| $\psi$ | level set function for liquid-solid interface |
| $\Omega$ | phase domain |
| $\Gamma$ | interface between phases |

**Subscripts**

| | |
|---|---|
| *f* | fluid |
| *int* | interface |
| *l* | liquid |
| *mic* | micro-region |
| *n* | nucleation |
| *s* | solid wall |
| *sat* | saturation |
| *v* | vapor |
| *w* | wall or waiting time |

## 1. INTRODUCTION

Nucleate boiling is one of the most efficient modes of heat transfer due to the latent heat of phase change, resulting in its wide applications for high heat flux transfer with limited superheat, like high energy electronic equipment and nuclear reactor. However, boiling is also a complex and elusive process. Thus, there isn't a consistent agreement on the mechanism of boiling heat transfer, and many empirical correlations and semi-mechanistic models for engineering applications flood in the literature up to now.

Recently, numerical simulation is used to study the local flow and heat transfer around growing bubble in this phenomenon. However, most of them [1-3] neglected the effect of the transient thermal response of the solid wall. For simplicity, a constant surface temperature is adopted instead of actual solid wall in numerical simulations [2-4]. Aktinol & Dhir [5] compared the cases with and without the solid wall under the same conditions. They found that, during the process of boiling, the surface temperature of solid wall can vary both temporally and spatially. Some authors [6] believed that the effect of the solid wall is necessary to be considered. Kenning & Yan [7] performed an experiments on bubble behaviors by thermochromic liquid crystal during nucleate pool boiling of water on a thin plate, and found that the bubble-driven heat removal is intrinsically unsteady and nonuniform. To measure the transient evolution of wall temperature underneath growing bubble, Fischer et al. [8] conducted boiling experiments in low gravity condition using the same technique of Kenning & Yan [7]. During the process of bubble growth, a local cold area with a distinct local temperature drop about 4 K can be observed, which moves with the three phase contact line. Mei et al. [9] analyzed the time scale required for the solid wall to adjust its temperature into a uniform distribution for most boiling systems, and found that it is much longer than the bubble growth time. Therefore, the actual bubble growth rate should be smaller than that predicted by a constant wall temperature.

Numerical simulation on bubble growth usually begins with an initial condition. Non-physical assumptions, however, were usually adopted for the initial flow and temperature fields. Furthermore, in order to eliminate the influence of non-physical assumptions of the initial conditions, multi-cycle simulation is necessary, and the nucleate criterion is needed to determine the appearance time for the subsequent bubble. Constant waiting time was used by some researchers [2, 10, 11], while the criterion of inception superheat at the cavity by Wang & Dhir [12]

was adopted by Aktinol and Dhir [5]. No comparison of the difference between different criteria has been made up to now.

In this paper, the influence of heater thermal capability on bubble thermal dynamics and heat transfer in single bubble pool boiling will be simulated numerically. The Ghost Fluid Method (GFM) is used for the sharp interface representation, while two level set functions are adopted for capturing the liquid-vapor-solid interfaces. Two nucleate criteria, i.e. constant waiting time and constant nucleate superheat for determining the appearance time for the subsequent bubble, are adopted, and the comparison between the predicted results is made to understand their influence. The transient thermal response of solid wall and its influence on bubble growth are also analyzed.

## 2. MATHEMATICAL MODEL

In the present study, the computational domain is divided into micro and macro regions (Fig. 1), which was initially proposed by Stephan & Hammer [1]. The micro region refers to the microlayer near three-phase contact line underneath the growing bubble, which has large contribution to the overall heat transfer and is dealt with by an independent model. The macro region, in which complete conservation equations of mass, momentum, and energy are solved, is the area occupied by vapor, liquid and solid around the bubble except the microlayer.

The following assumptions are made in the simulation: 1) the fluids in both phases are Newtonian, viscous and incompressible; 2) the material properties are constant in space and time and not influenced by the temperature and pressure; 3) the motion in fluid phases is axisymmetric and laminar; 4) the contact angle at the wall keeps constant; 5) the temperature is maintained constant at the bottom of solid wall.

The material properties of different phases are described by the Heaviside function with sharp interface representation as

$$\rho = \rho_s + \left(\rho_v + \left(\rho_l - \rho_v\right)H\left(\varphi\right) - \rho_s\right)H\left(\psi\right) \tag{1}$$

$$\mu = \mu_s + \left(\mu_v + \left(\mu_l - \mu_v\right)H\left(\varphi\right) - \mu_s\right)H\left(\psi\right) \tag{2}$$

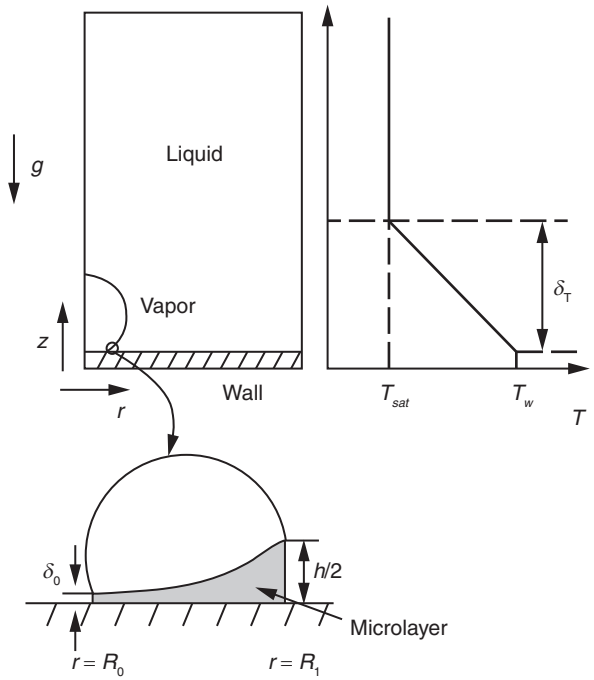


Figure 1: Computational domain used in numerical simulation.

$$k^{-1} = k_s^{-1} + \left(k_l^{-1} H(\varphi) - k_s^{-1}\right) H(\psi) \tag{3}$$

where $H$ is discontinuous Heaviside function which is described as below

$$H = \begin{cases} 1, & \text{if } \varphi \text{ or } \psi > 0 \\ 0, & \text{if } \varphi \text{ or } \psi \le 0 \end{cases} \tag{4}$$

The continuity, momentum, energy concentration conservation equations for the macro region are written as

$$\mathbf{u} = 0, \quad \Omega_s \tag{5}$$

$$\nabla \cdot \mathbf{u} = 0, \quad \Omega = \left\{\Omega_v \cup \Omega_l\right\} \tag{6}$$

$$\begin{aligned} \rho\left(\frac{\partial \mathbf{u}}{\partial t} + \mathbf{u} \cdot \nabla \mathbf{u}\right) &= -\nabla p + \nabla \cdot \mu(\nabla \mathbf{u} + \nabla \mathbf{u}^T) \\ &+ \rho\left[1 - \beta_T (T - T_{sat})\right] \boldsymbol{g}, \quad \Omega = \left\{\Omega_v \cup \Omega_l\right\} \end{aligned} \tag{7}$$

$$\begin{cases} \dfrac{\partial T}{\partial t} + \mathbf{u} \cdot \nabla T = \dfrac{1}{\rho C_p} \nabla \cdot k(\nabla T), & \Omega = \left\{\Omega_l \cup \Omega_s\right\} \\ T = T_{sat}(p_v), & \Omega_v \end{cases} \tag{8}$$

The conservation equations are solved accompany with the jump conditions [13, 14] at the interface

$$\left[\mathbf{u}\right]_\Gamma = \begin{cases} -\left[1/\rho\right]_\Gamma \dot{m}\mathbf{n}, & \Gamma_{lv} \\ 0, & \Gamma_{fs} \end{cases} \tag{9}$$

$$\left[\mu(\nabla u \cdot \mathbf{n}, \nabla v \cdot \mathbf{n}) \cdot \mathbf{t} + \mu(\nabla u \cdot \mathbf{t}, \nabla v \cdot \mathbf{t}) \cdot \mathbf{n}\right]_\Gamma = 0, \quad \Gamma_{lv} \tag{10}$$

$$\left[p\right]_\Gamma = 2\left[\mu(\nabla u \cdot \mathbf{n}, \nabla v \cdot \mathbf{n}) \cdot \mathbf{n}\right]_\Gamma - \sigma\kappa - \left[1/\rho\right]_\Gamma \dot{m}^2, \quad \Gamma_{lv} \tag{11}$$

$$\left[T\right]_\Gamma = 0, \quad \Gamma_{lv} \tag{12}$$

$$\left[k\nabla T \cdot \mathbf{n}\right]_\Gamma = \begin{cases} \dot{m}h_{fg}, & \Gamma_{lv} \\ 0, & \Gamma_{fs} \end{cases} \tag{13}$$

where the jump across the interface is defined as $\left[\Lambda\right]_\Gamma = \Lambda_l - \Lambda_v$, and the mass flux $\dot{m}$ is defined as $\dot{m} = \rho(\mathbf{u}_{\text{int}} - \mathbf{u}) \cdot \mathbf{n}$.

To non-dimensionalize the above equations, some characteristic scales for length and velocity are defined as $L = \sqrt{\dfrac{\sigma}{g(\rho_l - \rho_v)}}$ and $U = \sqrt{gL}$, while dimensionless temperature is defined as $\theta = \dfrac{T - T_{sat}}{T_w - T_{sat}}$.

In the micro region, one dimensional lubrication theory is adopted, which has been used and validated by a number of researchers in the literatures [1, 2, 9]. The combination of the mass, momentum, and energy equations for the micro-layer yields a fourth order differential equation

$$\delta'''' = f\left(\delta, \delta', \delta'', \delta'''\right) \tag{14}$$

According to the result of the equation (14), we can obtain the rate of vapor volume production from the micro region

$$\dot{V}_{mic} = \int_{R_o}^{R_1} \frac{k_l\left(T_w - T_{\text{int}}\right)}{\rho_v h_{fg} \delta \Delta V_{mic}} r\, dr \tag{15}$$

However, the solving process of equation (14) is very complex and time consuming. In the present paper, constant slope surface [15, 16] was adopted to derive the axisymmetric model, and the interface slope in the micro region is assumed to be

$$\frac{d\delta}{dr} = \tan\gamma \tag{15}$$

According to the above equations, the new formulation [4] of the micro region is obtained

$$q_{mic} = \frac{2\pi k_l\left(T_w - T_{sat}\right)}{\Delta A_{mic}} \left[ \begin{array}{l} \left(R_1 - \dfrac{h}{2\tan\gamma}\right) \dfrac{1}{\tan\gamma} \ln\left(\dfrac{h}{2}\dfrac{h_{ev}}{k_l} + 1\right) \\ + \dfrac{h}{2\tan^2\gamma} - \dfrac{k_l}{h_{ev}} \dfrac{1}{\tan^2\gamma} \ln\left(\dfrac{h}{2}\dfrac{h_{ev}}{k_l} + 1\right) \end{array} \right] \tag{17}$$

$$\dot{m}_{mic} = \frac{q_{mic}}{h_{fg}} \tag{18}$$

where $q_{mic}$ and $\dot{m}_{mic}$ are the area averaged heat flux and mass flux of the micro region respectively.

The following initial condition of velocity is used

$$u = v = 0 \tag{19}$$

while the initial temperature field in the whole domain is shown in Fig. 1. The thickness of initial thermal boundary layer is given by the following correlation [17]

$$\delta_T = 7.14\left(\frac{\nu_l \alpha_l}{g\beta_T \Delta T}\right)^{1/3} \tag{20}$$

Limited by the continuum hypothesis, the process of nucleation cannot be described in this numerical method. Thus, a new small bubble is placed on the solid wall when nucleate criterion is reached, which is similar to the bubble embryo motivated by artificial cavity. In the simulation,

initial radius of the small bubble is set to be $0.05L$. Criteria of constant waiting time and of constant nucleate superheat are chosen to determine its appearance. The Hsu's model [18] is adopted for the latter one, namely

$$\Delta T_n = T_w - T_{sat} = \frac{4 f_1 \sigma T_{sat}}{D_c h_{fg} \rho_v} \Big/ \left(1 - \frac{f_2 D_c}{2 f_1 \delta_T}\right) \tag{21}$$

where $f_1$ and $f_2$ are functions of the contact angle. Accordingly, if cavity size is given, corresponding nucleate superheat can be calculated by Eq. (21).

The computational domain of fluid was chosen to be $(1L, 2L)$ in order for that the bubble growth process is not affected by the computational boundary. The following boundary conditions are adopted for solving the conservation equations in the macro region, *i.e.*
at the axis of symmetry

$$u = \frac{\partial v}{\partial r} = \frac{\partial T}{\partial r} = \frac{\partial \varphi}{\partial r} = 0 \tag{22}$$

at the right of domain

$$u = \frac{\partial v}{\partial r} = \frac{\partial T}{\partial r} = \frac{\partial \varphi}{\partial r} = 0 \tag{23}$$

at the bottom of the wall

$$u = v = 0, T = T_W \tag{24}$$

at the top boundary

$$\frac{\partial u}{\partial z} = \frac{\partial v}{\partial z} = \frac{\partial \varphi}{\partial z} = 0, T = T_{sat} \tag{25}$$

Another two conditions in the wall also need to be considered

$$\left(k \frac{\partial T}{\partial z}\right)_{mic} = -q_{mic}, \quad \frac{\partial \varphi}{\partial z} = -\cos\gamma \tag{26}$$

## 3. NUMERICAL METHODS

For the macro region, the level set method (LSM) [19] is used for capturing the liquid-vapor-solid interfaces which separate the different phases.

The level set function $\varphi$ is defined as a signed distance from the liquid-vapor interface, where the interface location is the set of points where $\varphi = 0$, the liquid phase for $\varphi > 0$ and the vapor phase for $\varphi < 0$. It is advanced by solving the following equation

$$\frac{\partial \varphi}{\partial t} = -\mathbf{u}_{\text{int}} \cdot \nabla \varphi \tag{27}$$

where $\mathbf{u}_{int}$ is the interface velocity, defined as

$$\mathbf{u}_{\text{int}} = \frac{\dot{m}\mathbf{n}}{\rho} + \mathbf{u} \tag{28}$$

The unit surface normal and the surface curvature are defined as follows

$$\mathrm{n} = \frac{\nabla\varphi}{|\nabla\varphi|} \tag{29}$$

$$\kappa = \nabla.\mathbf{n} \tag{30}$$

Reinitialization is also needed to maintain a signed distance function from the interface

$$\varphi_\tau + S(\varphi_0)(1 - |\varphi|) = 0 \tag{31}$$

where smoothed out sign function $S(\varphi_0) = \dfrac{\varphi_0}{\sqrt{\varphi_0^2 + \Delta x^2}}$, $\varphi_0$ is a solution of Eq. (27).

Another level set function $\psi$ is used to treat the immersed solid surface which is defined as a signed distance from the fixed fluid-solid interface. The solid region refers to $\psi = < 0$, while fluid region to $\psi = > 0$. It is not necessary to be advanced. For more details of the level set method, including the related solving procedure and algorithm, one can refer to our former works [20, 21].

The ghost fluid method (GFM) [22] is employed for treating the jump conditions across the interface. Ghost fluid is created for one real fluid in the other fluid which keeps the discretization using values of only one kind fluid. The level set function is used to determine which values of the variable field corresponding to the real fluid and which to ghost fluid. Finally, the variables are extended into the entire domain. For example, the velocity and pressure of ghost fluid can be expressed as

$$\mathbf{u}^G = \mathbf{u} - [\mathbf{u}]_\Gamma \, sign(\varphi) \tag{32}$$

$$p^G = p - [p]_\Gamma \, sign(\varphi) \tag{33}$$

For more accurate computation, sub-cell location [16] of the interface is taken into account to discretize the derivative jump condition.

A standard MAC grid is used for spatial discretization where the velocities are defined at grid surfaces and other variables are defined at grid nodes. The projection method is used to numerically solve the Navier-Stokes equations. 2nd order ENO scheme is used for discretization of the convection term in momentum and energy equations, and central difference for diffusion terms. At the same time, ghost fluid method is used to deal with the sharp interface jump conditions.

## 4. MODEL VALIDATION

A comparison of the bubble growth process computed by the present numerical simulation is made with experimental data obtained by Siegel & Keshock [23] and numerical results without a solid wall simulated by Son [2]. The corresponding material parameters and nominal superheat on the bottom of solid wall are listed in Table 1, which is based on the conditions reported by Siegel & Keshock [23]. Considering that the thickness of solid wall used both in the experiment and in the present simulation is very thin ($h_w$=0.0127 mm) and its thermal diffusivity is very large, only one cycle of bubble growth is computed for saving time.

**Table 1. Material parameters and nominal superheat on the bottom of solid wall**

| Thermal diffusivity $\alpha$ ($\times 10^{-6}$ m$^2$/s) | | Contact angle $\gamma$ | Nominal superheat $\Delta T$ |
|---|---|---|---|
| **Water** | **Nickel (Ni)** | **(°)** | **(K)** |
| 0.35 | 19.49 | 38 | 6.17 |

Fig 2: shows the characteristics of bubble growth. The first row of Fig. 2a) shows the topological structures of bubble in some discrete time points corresponding to bubble incipience, growing, departure and rising up from the heating surface of solid wall, while the second row shows the evolutions of three phase contact point which is corresponded with bubble base. The results show that the prediction of bubble base diameter is a function of time with advancing and receding stages. Fig. 2b) shows temperature distributions on the heating surface for the five time points corresponding to those shown in Fig. 2a). It is obvious that a sharp temperature drop is observed clearly near the contact line during the bubble growth because of large evaporation in micro region. The temperature drop changes with the movement of contact line. After the bubble detached, the temperature drop disappears gradually and the temperature in the area affected by the movement of contact line begins to rise up because of the transient conduction of heater.

The temperature distributions along the center axis inside solid wall at five time points corresponding to those shown in Fig. 2a) are plotted in Fig. 3. It can be seen that the depth of thermal "hollow" is very small at the axis, and approximately linear profiles are presented in other area. This is mainly caused by the small thickness of solid wall, as well as the large difference of thermal diffusivity between solid wall and working fluid with magnitude of $O(10^2)$.

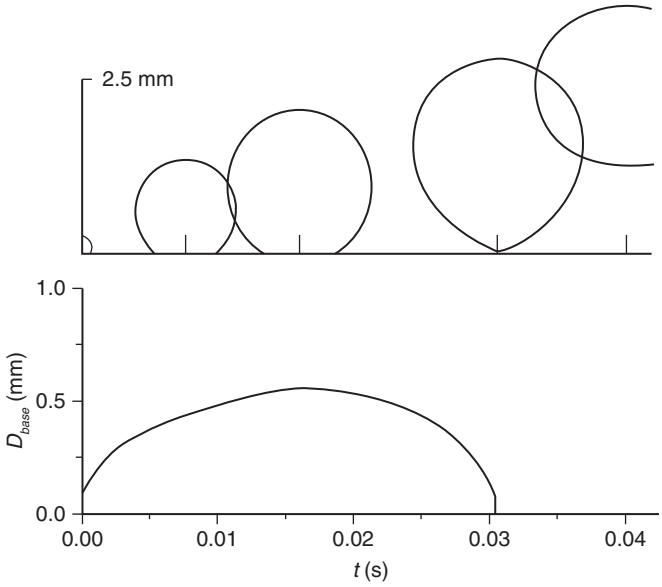


(a) Evolutions of the bubble shape and its base diameter

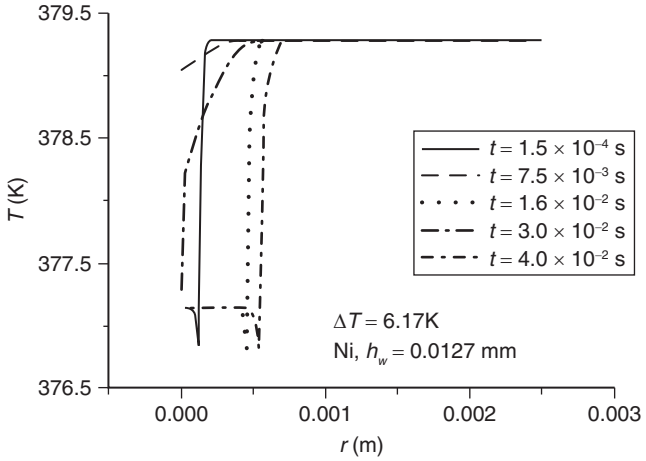


(b) Variations of temperature distribution on the upper surface of wall

Figure 2: Characteristics of bubble growth.

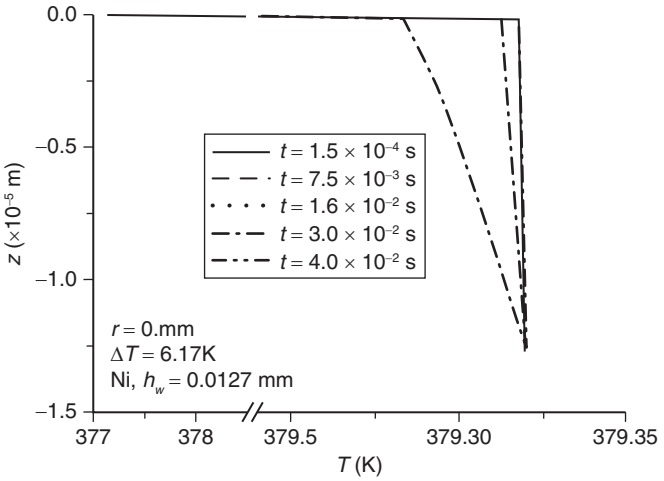


Figure 3: Variations of temperature distribution along the center axis.

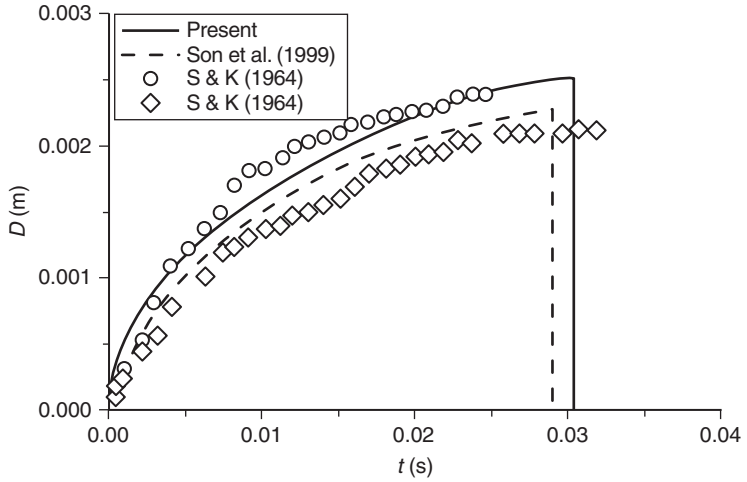


Figure 4: Comparison of bubble growth predicted by the present simulation with experimental data and other simulation.

Fig. 4 presents a comparison of the bubble growth predicted by the present numerical simulation experimental data obtained by Siegel & Keshock [23] and numerical results without a solid wall simulated by Son [2]. Good agreement is obvious. The predictions of bubble departure diameter and growth time are slightly bigger than Son's results, which is acceptable if one considers that the effect of transient thermal response of the solid wall is taken into account in the present numerical simulation. Fig. 5 shows the evolutions of area-averaged heat flux over the whole heating surface and that contributed by the micro region during the process of bubble growth. Generally, about 20 percent contribution is from the micro region to the total flux, which is also consistent quantitatively with the result of Son [2].

## 5. RESULTS AND DISCUSSION

Fig. 6 shows a typical multi-cycle process of a single bubble growing on nickel foil with thickness of 1 mm. Two nucleate criteria mentioned above are used, and the transition time is marked with the dashed lines. At first, the criterion of constant waiting time is used for determining the

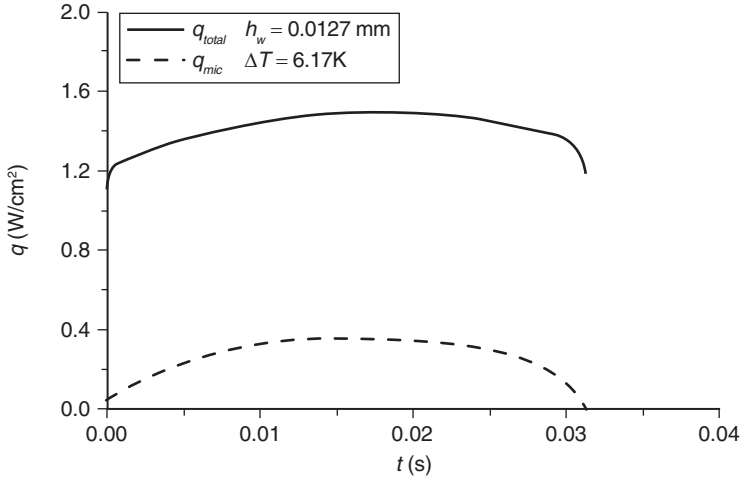


Figure 5: Evolutions of area-averaged heat flux over the whole heating surface and that contributed by the micro region during bubble growth.

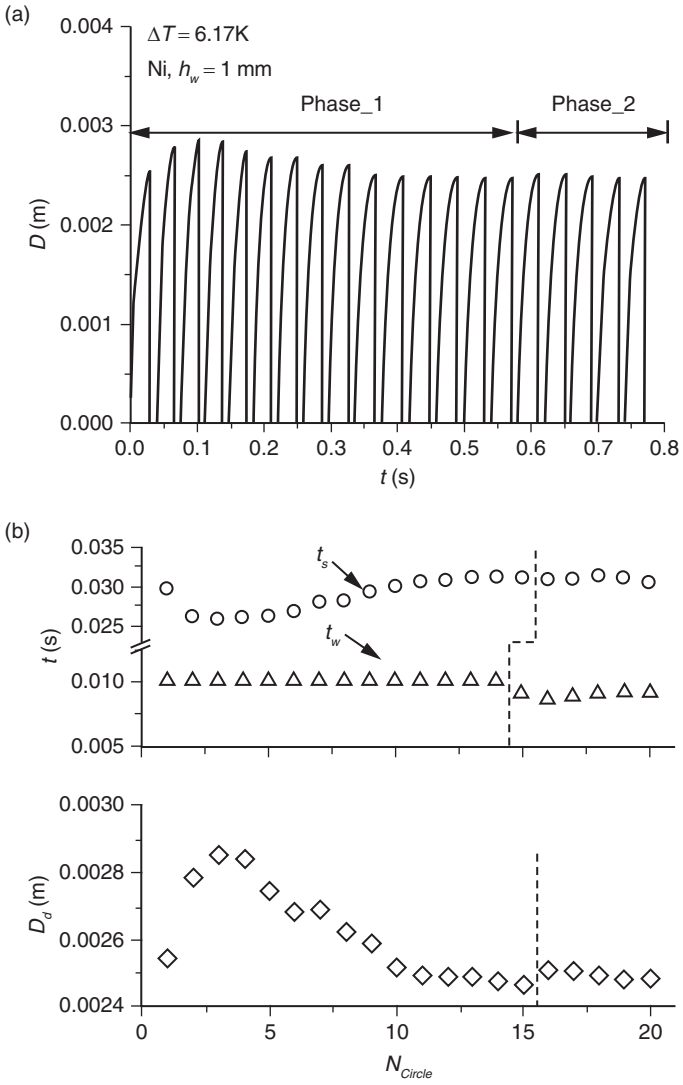


Figure 6: Typical multi-cycle process of bubble growth predicted by two different nucleate criteria.

appearance time for the subsequent bubble throughout Phase_1. A value of 10 ms is taken empirically as the waiting time. In Phase_2, the criterion of constant nucleate superheat is used instead of that of constant waiting time. The value of nucleate superheat is taken as 5.76 K, or correspondingly a cavity size of $7.1 \times 10^{-6}$ m based on Eq. (21). This value of nucleate superheat is obtained based on the predicted superheat at the nucleate site on the heating surface of solid wall at the beginning of the 14th cycle. Because a quasi-steady process of bubble growth is reached after the 11th cycle in Phase_1, the above values of waiting time and nucleate superheat can be considered as matched with each other. It is evident that a new quasi-steady process of bubble growth is reached after quick release transient stage from the 15th to 17th cycle. A comparison of characteristics of bubble growth between the predictions by the two different nucleate criteria, as well as that predicted in the 1st cycle, is shown in Fig. 7.

Firstly, the characteristic parameters, including departure diameter, growth time and waiting time, are approximately the same between the two quasi-steady processes of bubble growth predicted by the two different nucleate criteria, indicating their consistency in nature. However, the value of waiting time must be selected based on empirical database, which limits its applicability especially in cases without measured data. On the contrary, the criterion of nucleate superheat has a well-posed theoretical base, and then can be used in a wider range.

Secondly, a large difference exists between the 1st cycle and the quasi-steady processes of bubble growth. Furthermore, obvious variations of the characteristic parameters of bubble growth process are exhibited in the transient stage before the quasi-steady process of bubble growth is reached. The main reason for this phenomenon is the ideal but non-physical initial condition in the numerical simulation. Therefore, to eliminate the influence of eliminate on the process of bubble growth, multi-cycle simulation is necessary.

Fig. 8 shows the evolutions of bubble topological structure, temperature and flow fields during a typical cycle in Phase_2. It can be observed clearly that a fast bubble growth exists in the beginning of the bubble cycle, caused by the energy stored both in the thermal boundary layer of liquid adjacent to the heating surface and in solid wall underneath the growing bubble. The interface is expanded in the radial directions, and then the contact line advances to enlarge the bubble base. Along with the bubble growth, the gradient of temperature around the interface descents, eventually leading to a lower and lower bubble growth rate, especially when bubble grows out of the thermal boundary layer. As the buoyancy force becomes large enough, bubble will rise up and then the contact line will be pulled back until the bubble departing from the heating surface. A vortex is generated when the contact line recedes, which promotes the fresh liquid flowing towards the bottom of the growing bubble and quickens the bubble rising up. A clear

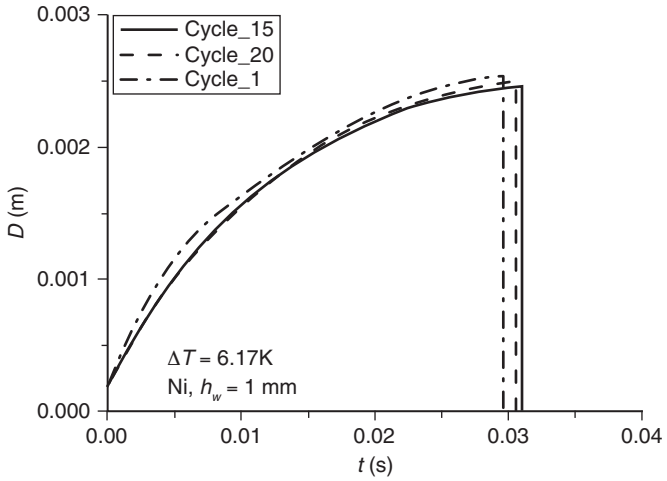


Figure 7: Comparison of characteristics of bubble growth predicted by different nucleate criteria.

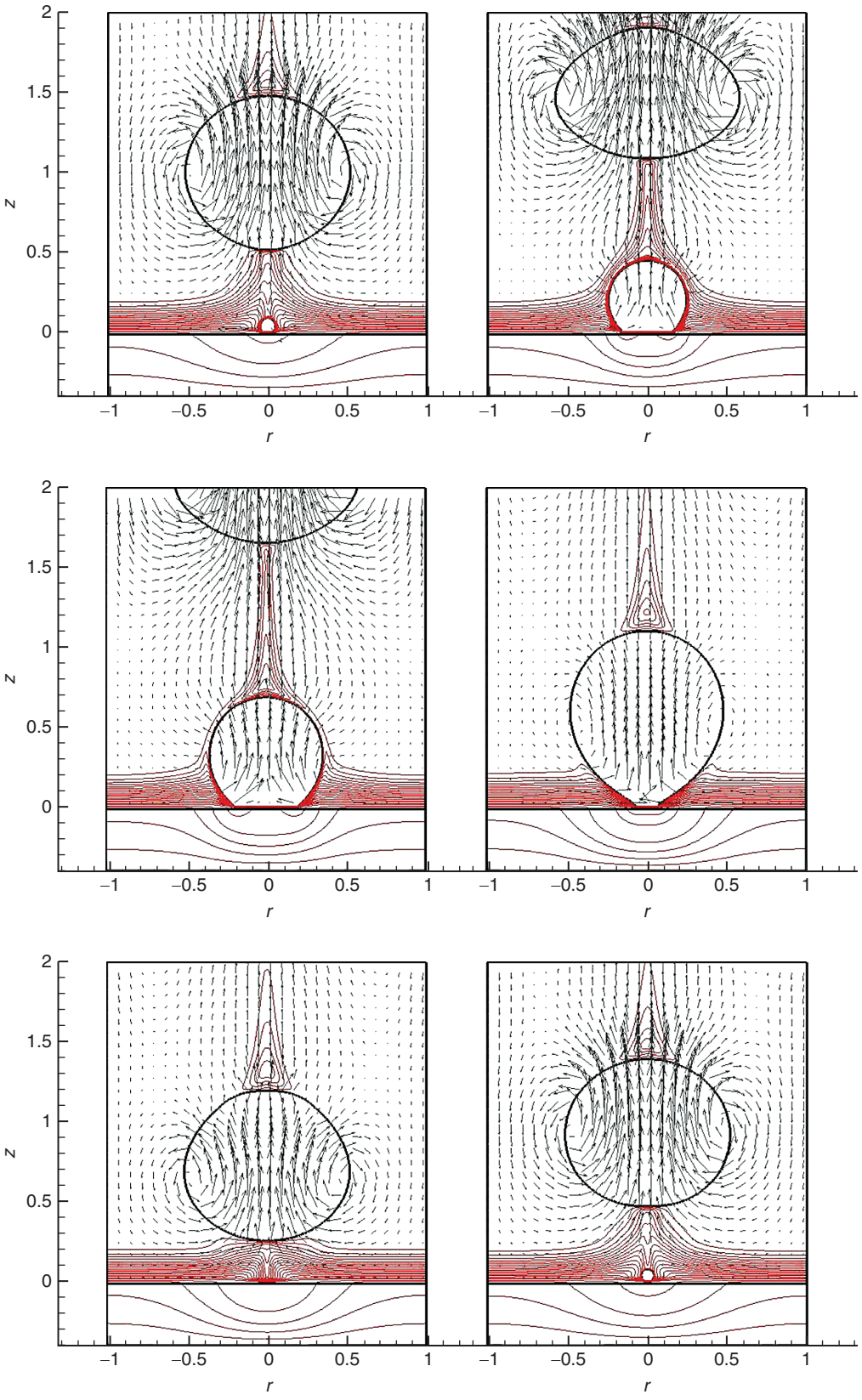


Figure 8: Evolutions of bubble topological structure, temperature and flow fields during a typical quasi-steady bubble cycle (interval of isotherm: 0.05 for 0~0.95 inside fluid while 0.01 for 0.97~1 inside solid wall).

thermal "hollow" is produced inside the solid wall underneath the bubble base, which has a periodical expanding and receding feature because of the movement of contact line, and relevant evaporation of microlayer and transient heat conduction inside solid wall. It is also obvious that the recovery of the temperature on the nucleate site and the thermal boundary layer near the heating surface is influenced by heat conduction inside solid wall, and then the transient heat transfer and the periodical thermal storing and releasing of solid wall can affect evidently bubble thermal dynamics and heat transfer.

Fig. 9 shows the variations of local temperature and corresponding heat flux at different locations inside solid wall during the typical cycle in Phase_2 shown in Fig. 8. Here, $\Delta h_{surface}$ denotes the distance from the heating surface, while $r$ the distance from the nucleate site. Twice sharp temperature drops can be observed clearly during bubble growth, which are caused by strong evaporation of microlayer near the contact line. The closer the point locates to the nucleate site, the bigger the temperature drop is. It is also observed that the temperature drop, as well as the corresponding peak of heat flux, is prolonged and weakened with the depth inside solid wall. Only

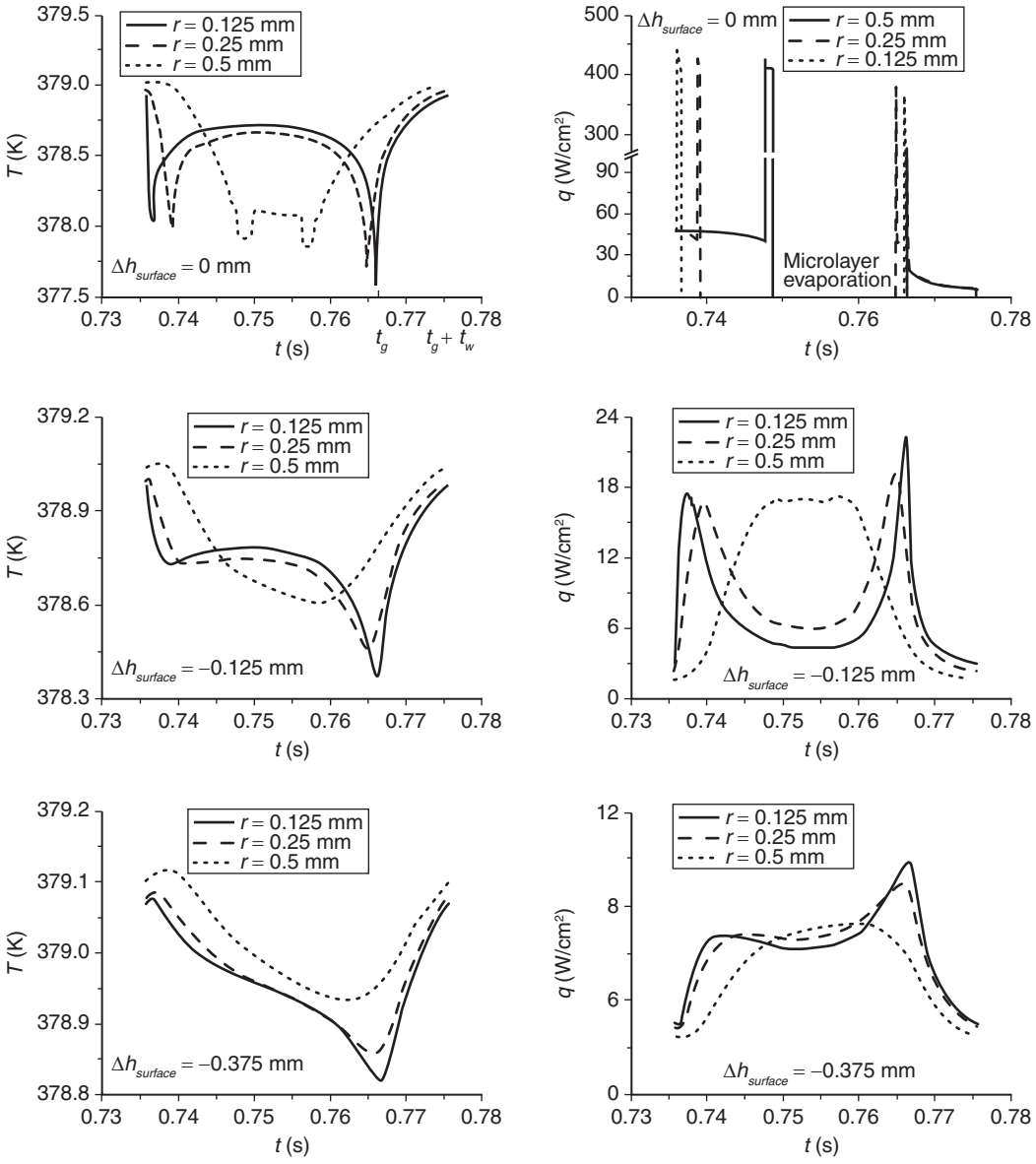


Figure 9: Variations of temperature and heat flux at different locations inside solid wall.

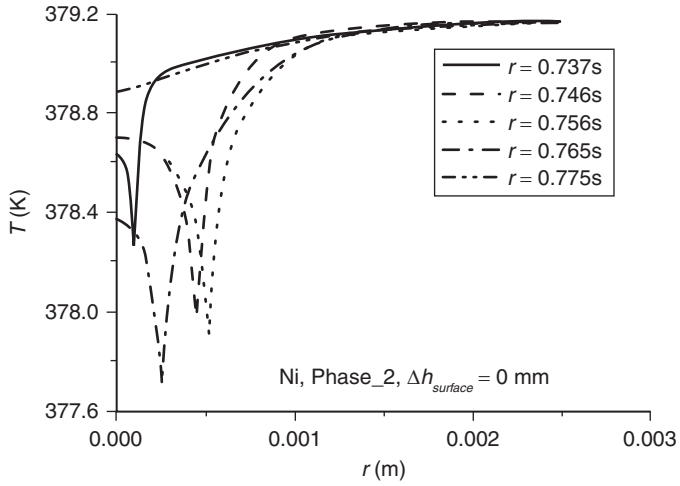


Figure 10: Evolutions of temperature distribution on heating surface.

once obvious drop of temperature is even observed if the depth is large enough as shown in Fig. 9c). This is mainly because of the transient thermal response of solid wall. After bubble departure, the temperature inside solid wall in the vicinity of nucleate site is recovered by fresh liquid re-flooding the local dry spot and by the transient heat conduction inside solid wall. A qualitative agreement can be found between the present numerical prediction and the experimental measurement by Moghaddam & Kiger [24].

Fig. 10 shows the evolutions of temperature distribution on the heating surface during the same typical cycle. As mentioned earlier, the local temperature drop moves with the movement of the contact line. Besides, there is no clear variation far away from the center axis, which versifies in some sense that the computational domain is large enough to prevent the spurious influence of boundaries.

## 6. CONCLUSIONS

The complete process of single bubble growth including the transient thermal response of solid wall is simulated numerically with sharp interface representation. The numerical results agree well with other numerical and experimental results under similar conditions. It is also shown that the ideal but non-physical initial conditions used in numerical simulation deeply affect the process of bubble growth. Multi-cycle simulation is necessary to eliminate this influence.

Two nucleate criteria, namely constant waiting time and constant nucleate superheat, are used for determining the appearance time for the subsequent bubble. Quasi-steady process of bubble growth can always reach after a transient release stage in both cases. The characteristic parameters, including departure diameter, growth time and waiting time, are approximately the same between the two quasi-steady processes of bubble growth predicted by the two different nucleate criteria, indicating their consistency in nature.

The temperature on the heating surface and inside solid wall may vary temporally and spatially. A periodically expanding and receding thermal “hollow” can be observed inside solid wall underneath the growing bubble. The recovery of the temperature on the nucleate site and the thermal boundary layer near the heating surface is influenced by heat conduction inside solid wall, and then the transient heat transfer and the periodical thermal storing and releasing of solid wall can affect evidently bubble thermal dynamics and heat transfer.

## ACKNOWLEDGE

The present study is supported financially by the National Natural Science Foundation of China under the grants of 11372327 and 10972225, and the Strategic Priority Research Program on Space Science, the Chinese Academy of Sciences under the grants of XDA04020404 and XDA04020202-04. The authors also appreciate Prof. Li Yuan (Academy of Mathematics and Systems Science, CAS), and Prof. Zai-Sha Mao (Institute of Process Engineering, CAS) for fruitful discussions.

## REFERENCES


[1] Stephan, P. and Hammer, J., A new model for nucleate boiling heat transfer, *Heat and Mass Transfer*, 1994, 30(2), 119–125.

[2] Son, G., Dhir, V.K. and Ramanujapu, N., Dynamics and heat transfer associated with a single bubble during nucleate boiling on a horizontal surface, *Journal of Heat Transfer*, 1999, 121, 623–631.

[3] Dhir, V.K., Mechanistic prediction of nucleate boiling heat transfer-achievable or a hopeless task? *ASME Journal of Heat Transfer*, 2006, 128(1), 1–12.

[4] Zhao, J.F., Li, Z.D. and Zhang, L., Numerical simulation of single bubble pool boiling in different gravity conditions, *New Trends in Fluid Mechanics Research / Proceeding of 6th International Conference on Fluid Mechanics*, Guangzhou, China, June 30-July 3, 2011.

[5] Aktinol, E. and Dhir, V.K., Numerical simulation of nucleate boiling phenomenon coupled with thermal response of the solid, *Microgravity Science and Technology*, 2012, 24, 255–265.

[6] Zhang, L. and Zhao, J.F., Influence of heater thermal capacity on pool boiling heat transfer, *International Conference on Multiphase Flow 2013*, Jeju, Korea, May 26–31, 2013.

[7] Kenning, D.B.R. and Yan, Y., Pool boiling heat transfer on a thin plate: features revealed by liquid crystal thermography, *International Journal of Heat and Mass Transfer*, 1996, 39(15), 3117–3137.

[8] Fischer, S., Herbert, S., Sielaff, A., Slomski, E.M., Stephan, P. and Oechsner, M., Experimental investigation of nucleate boiling on a thermal capacitive heater under variable gravity conditions, *Microgravity Science and Technology*, 2012, 24(3), 139–146.

[9] Mei, R., Chen, W. and Klausner, J.F., Vapor bubble growth in heterogeneous boiling-I. Formulation, *International Journal of Heat and Mass Transfer*, 1995, 38(5), 909–919.

[10] Son, G. and Dhir, V.K., Numerical simulation of nucleate boiling on a horizontal surface at high heat fluxes, *International Journal of Heat and Mass Transfer*, 2008, 51, 2566–2582.

[11] Kunkelmann, C. and Stephan, P., Numerical simulation of the transient heat transfer during nucleate boiling of refrigerant HFE-7100, *International Journal of Refrigeration*, 2010, 33, 1221–1228.

[12] Wang, C.S. and Dhir, V.K., Effect of surface wettability on active nucleation site density during pool boiling of water on vertical surface, *Journal of Heat Transfer*, 1993, 115, 659–669.

[13] Nguyen, D.Q., Fedkiw, R.P. and Kang, M., A boundary condition capturing method for incompressible flame discontinuities, *Journal of Computational Physics*, 2001, 172(1), 71–98.

[14] Liu, X.D., Fedkiw, R.P. and Kang, M., A boundary condition capturing method for Poisson's equation on irregular domains, *Journal of Computational Physics*, 2000, 160, 151–178.

[15] Son, G., Numerical study on a sliding bubble during nucleate boiling, *KSME International Journal*, 2001, 15(7), 931–940.

[16] Jung, S. and Kim, H., Synchronized measurement of liquid-vapor phase and temperature distributions on a boiling surface during single bubble nucleate boiling, Jeju, Korea, *8th International Conference on Multiphase Flow*, May 26-31, 2013.

[17] Kays, W.M. and Grawford, M.E., Convective Heat and Mass Transfer, McGraw-Hill, New York, 1980.

[18] Hsu, Y.Y., On the size range of active nucleation cavities on a heating surface, *ASME Journal of Heat Transfer*, 1962, 84, 207–216.

[19] Osher, S. and Fedkiw, R., Level Set Methods and Dynamic Implicit Surfaces. Springer-Verlag, New York, 2003.

[20] Zhao, J.F., Li, Z.D., Li, H.X. and Li, J., Thermocapillary migration of deformable drops at moderate to large marangoni number in microgravity, *Microgravity Science and Technology*, 2010, 22(3), 295–303.

[21] Zhao, J.F., Zhang, L., Li, Z.D. and Qin, W.T., Topological structure evolvement of flow and temperature fields in deformable drop marangoni migration in microgravity, *International Journal of Heat and Mass Transfer*, 2011, 54, 4655–4663.

[22] Fedkiw, R.P., Aslam, T., Merriman, B. and Osher, S., A non-oscillatory eulerian approach to interfaces in multimaterial flows (the Ghost Fluid Method), *Journal of Computational Physics*, 1999, 152(2), 457–492.

[23] Siegel, R. and Keshock, E.G., Effects of reduced gravity on nucleate boiling bubble dynamics in saturated water, *AIChE Journal*, 1964, 10(4), 509–516.